

**OPEN ACCESS**

## The $\mu$ -RWELL layouts for high particle rate

To cite this article: G. Bencivenni *et al* 2019 *JINST* **14** P05014

View the [article online](#) for updates and enhancements.

### Recent citations

- [Production and performance study of Diamond-Like Carbon resistive electrode in MPGD](#)  
You Lv *et al*



**IOP | ebooks™**

Bringing you innovative digital publishing with leading voices to create your essential collection of books in STEM research.

Start exploring the collection - download the first chapter of every title for free.

## The $\mu$ -RWELL layouts for high particle rate

**G. Bencivenni,<sup>a,1</sup> R. de Oliveira,<sup>b</sup> G. Felici,<sup>a</sup> M. Gatta,<sup>a</sup> M. Giovannetti,<sup>a</sup> G. Morello,<sup>a</sup>  
A. Ochi,<sup>c</sup> M. Poli Lener<sup>a</sup> and E. Tskhadadze<sup>a,d</sup>**

<sup>a</sup>Laboratori Nazionali di Frascati dell'INFN,  
Via E. Fermi 40, Frascati, Italy

<sup>b</sup>CERN,  
Esplanade des Particules 1, Meyrin, Switzerland

<sup>c</sup>Kobe University,  
1-1 Rokkodai-cho, Nada-ku, Kobe 657-8501, Japan

<sup>d</sup>Technological Institute of Georgia,  
39-A Chavchavadze Ave., 0179 Tbilisi, Georgia

E-mail: [giovanni.bencivenni@lnf.infn.it](mailto:giovanni.bencivenni@lnf.infn.it)

**ABSTRACT:** The  $\mu$ -RWELL is a single-amplification stage resistive Micro-Pattern Gaseous Detector (MPGD). The detector amplification element is realized with a single copper-clad polyimide foil micro-patterned with a blind hole (well) matrix and embedded in the readout PCB through a thin Diamond-Like-Carbon (DLC) sputtered resistive film. The introduction of the resistive layer, suppressing the transition from streamer to spark, allows to achieve large gains ( $\geq 10^4$ ) with a single amplification stage, while partially reducing the capability to stand high particle fluxes. The simplest resistive layout, designed for low-rate applications, is based on a single-resistive layer with edge grounding. At high particle fluxes this layout suffers of a non-uniform response. In order to get rid of such a limitation different current evacuation geometries have been designed. In this work we report the study of the performance of several high rate resistive layouts tested at the CERN H8-SpS and PSI  $\pi$ M1 beam test facilities. These layouts fulfill the requirements for the detectors at the HL-LHC and for the experiments at the next generation colliders FCC-ee/hh and CepC.

**KEYWORDS:** Particle tracking detectors (Gaseous detectors); Time projection chambers

<sup>1</sup>Corresponding author.

---

## Contents

<b>1</b>	<b>Introduction</b>	<b>1</b>
<b>2</b>	<b>The Diamond-Like-Carbon</b>	<b>3</b>
<b>3</b>	<b>The high rate layouts</b>	<b>3</b>
3.1	The Double-Resistive layout	4
3.2	The Silver-Grid layout	5
<b>4</b>	<b>Performance of the HR-layouts</b>	<b>7</b>
4.1	Efficiency studies	8
4.2	Rate capability measurement	10
4.3	Discharge studies	10
<b>5</b>	<b>Conclusions</b>	<b>12</b>
<b>A</b>	<b>A model for HR-layouts</b>	<b>13</b>

---

## 1 Introduction

The  $\mu$ -RWELL, figure 1, is a single-amplification stage resistive MPGD [1] that combines in a unique approach the solutions and improvements achieved in the last years in the MPGD field. The R&D on  $\mu$ -RWELL aims to improve the stability under heavy irradiation while simplifying the construction procedures in view of an easy technology transfer to industry: a milestone for large scale applications in fundamental research at the future colliders and even beyond the HEP.

The detector is composed of two elements: the cathode, a simple FR4 PCB with a thin copper layer on one side and the  $\mu$ -RWELL\_PCB, the core of the detector. The  $\mu$ -RWELL\_PCB, a multi-layer circuit realized by means of standard photo-lithography technology, is composed of a well patterned single copper-clad polyimide (Apical<sup>®</sup>) foil<sup>1</sup> acting as amplification element of the detector; a resistive layer, realized with a DLC film sputtered on the bottom side of the polyimide foil, as discharge limitation stage; a standard PCB for readout purposes, segmented as strip, pixel or pad electrodes.

Applying a suitable voltage between the copper layer and the DLC, the well acts as a multiplication channel for the ionization produced in the drift gas gap, figure 2. The charge induced on the resistive film is spread with a time constant [2, 3]

$$\tau = \rho c = \rho \frac{\epsilon_0 \epsilon_r}{t}$$

being  $\rho$  the surface resistivity (in the following simply called resistivity),  $c$  the capacitance per unit area and  $t$  the distance between the resistive layer and the readout plane.

---

<sup>1</sup>50  $\mu$ m thick polyimide covered on one side with 5  $\mu$ m thick copper, similar to the GEM base material.

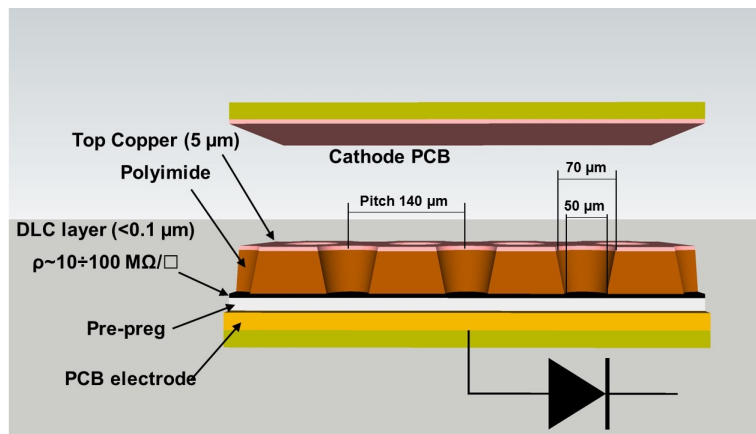


Figure 1. Layout of the  $\mu$ -RWELL.

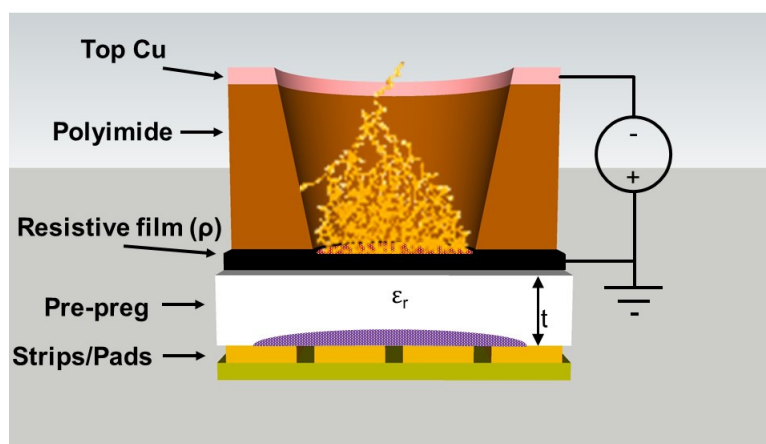


Figure 2. Principle of operation of the  $\mu$ -RWELL.

The spark suppression mechanism is similar to the one of the Resistive Plate Counters — RPCs, [4–7]: the streamer created inside the amplification volume, inducing a large current flowing through the resistive layer, generates a localized drop of the amplifying voltage with an effective quenching of the multiplication process in the gas. This mechanism strongly suppressing the discharge amplitude allows an operation of the detector at large gains ( $\geq 10^4$ ) with a single amplification stage.

A drawback, correlated with the Ohmic behaviour of the detector, is the reduced capability to stand high particle fluxes. Indeed a detector relying on a simple single-resistive layout suffers at high particle fluxes of a non-uniform response over its surface, more evident as the size of the detector increases. This effect, correlated to the average resistance ( $\Omega$ ) faced by the charge produced in the avalanche, actually depends on the distance between the particle incidence position and the detector grounding line.

In this paper we discuss the resistive layouts for high rate purposes and their performance in terms of efficiency and rate capability as measured in different beam conditions at the CERN and PSI beam lines.

## 2 The Diamond-Like-Carbon

The DLC sputtering technology is typically used in applications (mechanics, automotive and medical industry) that require surface hardening and reduced abrasive wear. The sputtered DLC is a class of carbon material that contains both the diamond as well as the graphite structure.

For the production of our detectors, a large industrial sputtering chamber in Be-Sputter Co., Ltd. (Japan) has been used [8]. Starting from a target of graphite, magnetron-sputtered on one side of the Apical<sup>®</sup> foil, the DLC film is eventually obtained with suitable surface resistivity and uniform thickness. The resistivity dependence as a function of the DLC thickness for different sputtering batches is shown in figure 3. The black calibration curve has been obtained by sputtering the DLC on a brand-new Apical<sup>®</sup> foil, while the open square markers refer to the  $\mu$ -RWELL 2017 test production done on a pre-dried base material (200°C for ~2 hours).

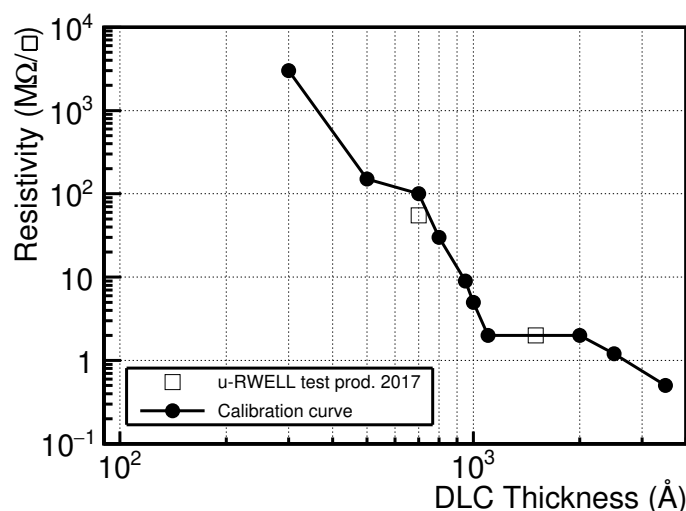


**Figure 3.** Resistivity as a function of the DLC thickness for different sputtering batches [9].

Very recent developments [10] at USTC-Hefei (PRC) led to the manufacturing of DLC+Cu sputtered Apical<sup>®</sup> foils, where additional few microns of copper cover the free surface of the DLC layer. This technology opens the way towards improved high rate  $\mu$ -RWELL layouts.

## 3 The high rate layouts

The simplest scheme for the evacuation of the current in a  $\mu$ -RWELL is based on a single resistive layer with a grounding line all around the active area, figure 4, (Single-Resistive layout — SRL). For large area devices the path of the current to ground could therefore be large and strongly dependent on the incidence point of the particle.

In order to cope with this effect the solution is to reduce as much as possible the average path towards the ground connection, introducing a high density grounding network on the resistive stage.

Two different high rate (HR) layouts with dense grounding scheme have been implemented: the Double-Resistive Layer (DRL) and the Silver-Grid (SG).

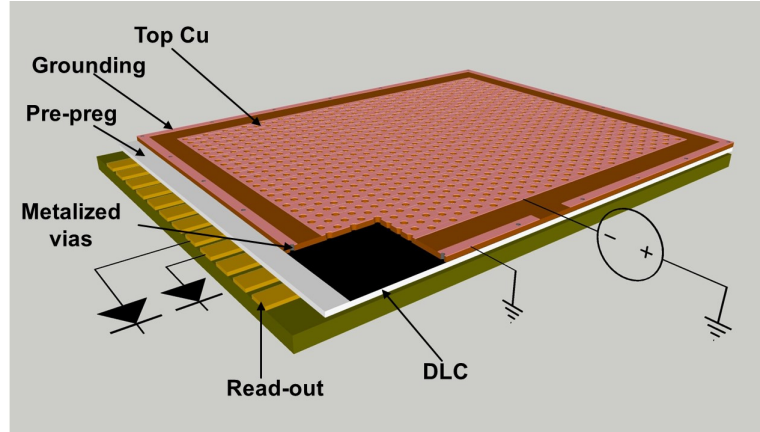


Figure 4. Sketch of the Single-Resistive layout.

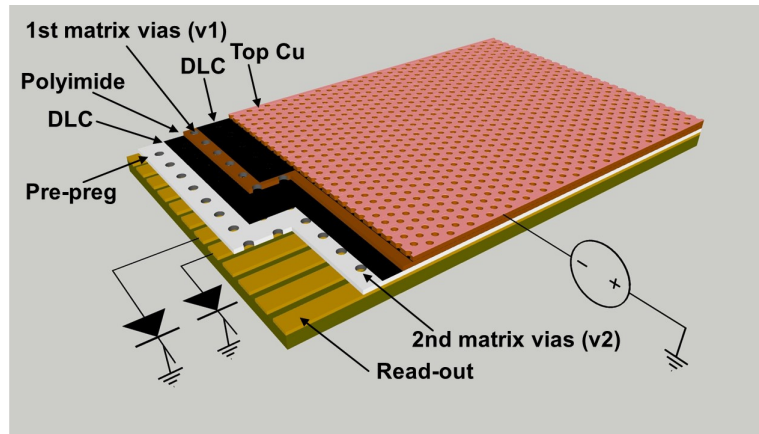
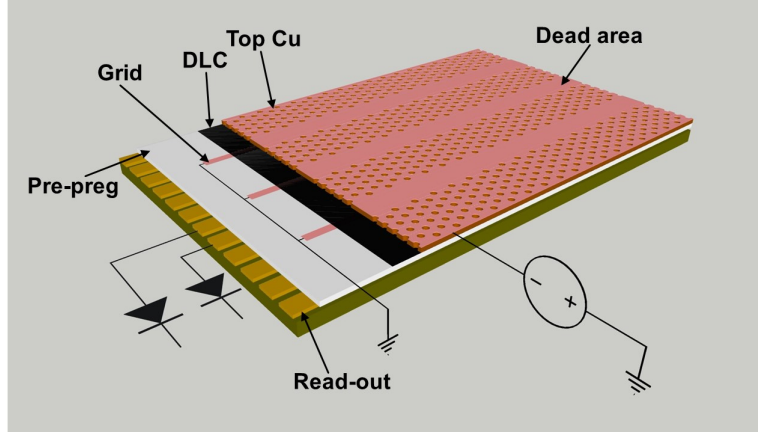


Figure 5. Sketch of the Double-Resistive layout.

### 3.1 The Double-Resistive layout

The DRL layout is sketched in figure 5. The first DLC film, sputtered on the back-plane of the amplification stage, is connected to a second DLC layer by means of a matrix of metalized vias (v1). A further matrix of vias (v2) connects the second DLC film to the underlying readout electrodes, providing the final grounding of the whole resistive stage. The vias density is typically  $\leq 1 \text{ cm}^{-2}$ . In this way a 3D-current evacuation layout is obtained and the average resistance,  $\Omega_{\text{DRL}}$ , seen by the current is minimized with respect to the  $\Omega_{\text{SRL}}$  of the SRL scheme, just for geometry and Ohm's law considerations. In appendix A we refer to a model explaining this effect in the particular case of point-like irradiation at the center of the basic cell.

Since the technology transfer of the DRL industrial production is difficult, a new simplified resistive scheme for high particle rate purposes has been developed. The new design, described in detail in the next section, is based on the simple single-resistive layout with a suitable surface current evacuation scheme.



**Figure 6.** Sketch of the Silver-Grid layout.

### 3.2 The Silver-Grid layout

The Silver-Grid (SG) layout, is sketched in figure 6. The conductive grid deposited on the DLC layer acts as a high density 2-D current evacuation system. The pitch of the grid together with the resistivity of the DLC,  $\rho$ , are parameters of this layout. In the first prototypes the conductive grid has been screen-printed using a silver paste, from which the name of the layout.

The presence of a conductive grid on the DLC can induce discharges over its surface, figure 7a. This effect, depending on the resistivity, requires the introduction of a small dead zone in the amplification stage above the grid lines (see figure 6). In order to properly size the dead zone, a study of the surface discharges on the DLC has been performed. For this purpose a custom tool, figure 7b, composed of two movable thin conductive tips has been built. The tips are placed in contact with the DLC and supplied with HV. The distance between the two tips can be gauged with a micrometric screw. In figure 9 the *distance-of-closest-approach* (DOCA) before the occurrence of a discharge is reported as a function of the DLC resistivity for different voltages. In all the  $\mu$ -RWELL layouts the DOCA can be defined as the minimum distance between a grounding line and the closest well.

In a simplified model of the resistive layouts the charge moving on the DLC would experience an effective resistance  $\Omega_{\text{eff}}$  that we define as:

$$\Omega_{\text{eff}} = \frac{\rho (\text{pitch}/2 + \text{DOCA})}{2w} \quad (3.1)$$

The  $\Omega_{\text{eff}}$  comes from the definition of the surface resistance,  $\rho$ , that is applicable in general to resistive films such as our DLC. Considering a thin portion of the DLC (figure 8), with length  $L$  and width  $w$ , the resistance is  $R = \rho (L/w)$ . In our estimate we have considered that  $w = 1 \text{ mm}$ . Under these assumptions, considering the approximation that the basic cell of the detector is uniformly irradiated we obtain the  $\Omega_{\text{eff}}$ .<sup>2</sup> For the DRL layout the DOCA is the distance between a vias  $v_1$  and the closest vias  $v_2$ , while the pitch is the distance between two closest vias  $v_1$  (section 3.1). For the SRL, being essentially a large SG, the pitch is half of the detector edge.

---

<sup>2</sup> $\Omega_{\text{eff}} = \frac{\rho}{w} \left( \int_{\text{DOCA}}^{\text{pitch}/2} x dx \right) \left( \int_{\text{DOCA}}^{\text{pitch}/2} dx \right)^{-1}$ .

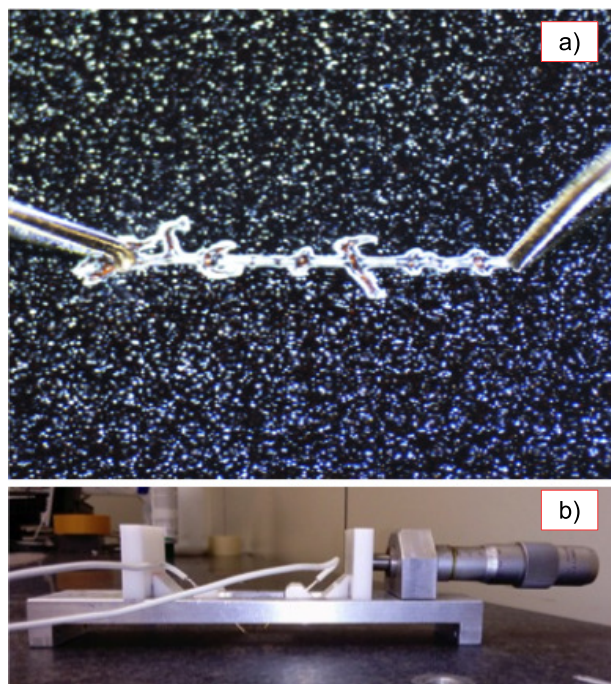


**Figure 7.** a) the effect of a discharge on the DLC surface; b) the tool used for the study of the discharges on the DLC surface.

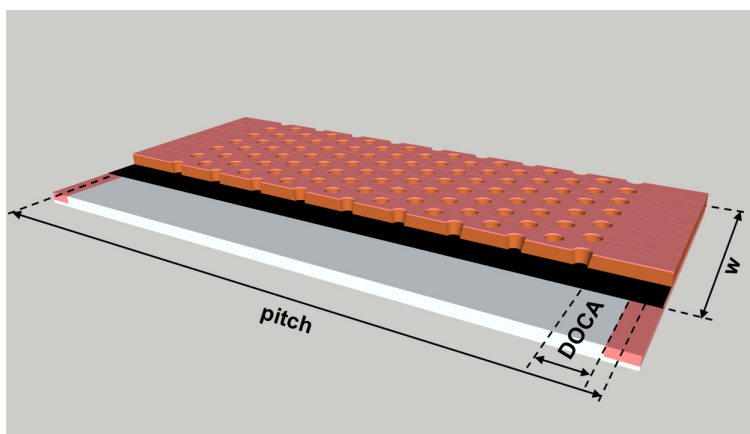


**Figure 8.** Cross-section of a Silver Grid layout with the definition of its parameters.

It is worth pointing out how the  $\Omega_{\text{eff}}$  is different from the  $\Omega$  mentioned in appendix A: the second one actually is defined for point-like irradiation at the centre of the detector basic cell.

In table 1 we report the characteristics of the HR-layouts described in this work. For completeness also the parameters of the SRL have been included.

The SG layouts exhibit a geometrical acceptance lower than the other detectors because of the presence of dead zone. Thanks to the DLC+Cu technology, allowing the photo-etching of very thin grid lines ( $\approx 100 \mu\text{m}$  width), for the SG2++ it has been possible to reduce the dead zone down to 5% of the active area.



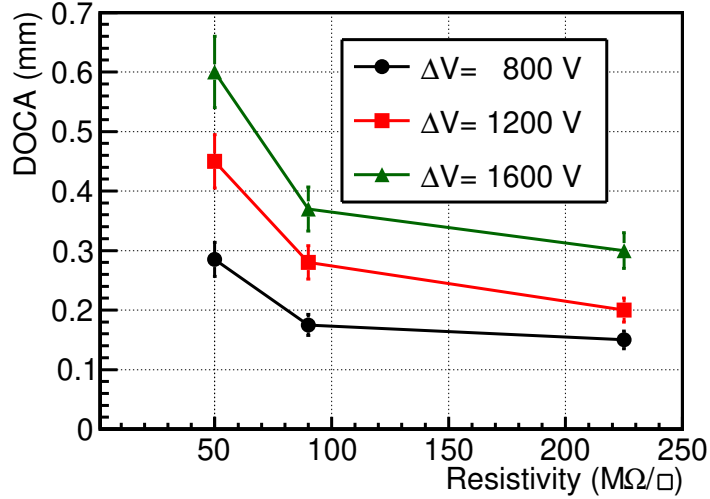


**Figure 9.** DOCA vs DLC resistivity for different voltages applied to the tips.

**Table 1.** Resistive and geometrical parameters of the HR-layouts compared with the low rate baseline option (SRL). For the SG models the ground-pitch is the grid-pitch.

Layout	$\rho$ (MΩ/□)	ground-pitch (mm)	dead-zone (mm)	DOCA (mm)	geometric acceptance (%)	$\Omega_{\text{eff}}$ (MΩ)
SG1	70	6	2	0.85	66	134
SG2	65	12	1.2	0.45	90	209
SG2++	64	12	0.6	0.25	95	200
DRL	54	6	0	7	100	270
SRL	70	100	0	5.5	100	1947

#### 4 Performance of the HR-layouts

The performance of the HR-layouts have been measured with pion and muon beams at the H8-SpS of CERN and the  $\pi$ M1 of PSI. The experimental set-up used in both beam tests is composed of:

- two couple of plastic scintillators (up-stream/down-stream), providing the DAQ trigger
- two external triple-GEM trackers equipped with 650  $\mu\text{m}$  pitch X-Y strip read-out with analog APV25 front-end electronics [13], defining the particle beam with a spatial accuracy of the order of 100  $\mu\text{m}$
- six  $\mu$ -RWELL detectors based on different resistive layouts, equipped with  $0.6 \times 0.8 \text{ cm}^2$  pads and read-out with APV25 and current monitored

The gaseous detectors have been operated with Ar/CO<sub>2</sub>/CF<sub>4</sub> (45/15/40) gas mixture.

The relevant physical quantities are reported in this paper as a function of the detector gas gain<sup>3</sup> to take into account small manufacturing differences in the amplification stage of the  $\mu$ -RWELL

<sup>3</sup>The gain of a gaseous detector is defined as the multiplication factor of the total ionization generated by a particle crossing the gas conversion gap. Therefore it can be estimated as the ratio between the average collected charge Q and the total ionization charge.

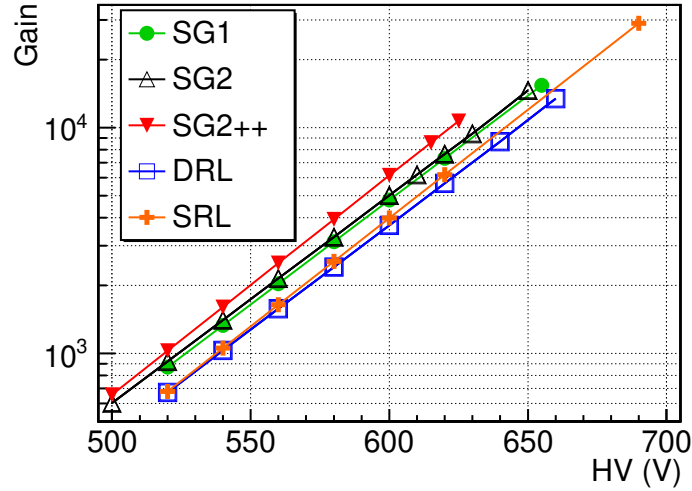


**Figure 10.** Gas gain of the detectors characterized at PSI. The maximum value of the gain could be correlated with the different measurement conditions in terms of particle flow.

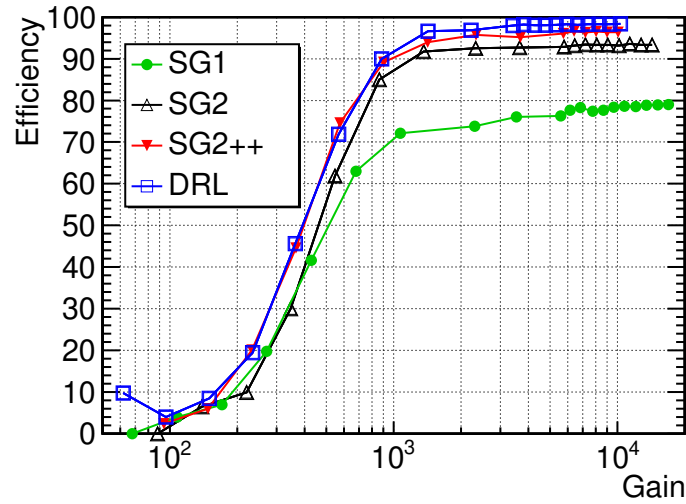


**Figure 11.** Efficiency as a function of the gas gain for the HR layouts.

prototypes (i.e. well diameter and shape). In figure 10 we plot the gas gain of all prototypes measured with a 270 MeV/c  $\pi^+$  beam at PSI, with particle fluxes ranging from  $\sim 300$  kHz/cm<sup>2</sup> up to  $\sim 1.2$  MHz/cm<sup>2</sup> well below the onset of the Ohmic drop of the detectors gain (see section 4.2).

#### 4.1 Efficiency studies

In figure 11 the efficiency of the HR-layouts is reported as a function of the detectors gain. The measurement has been performed with a flux of  $\sim 300$  kHz/cm<sup>2</sup>  $\pi^-$  (350 MeV/c) and an average beam spot of  $5 \times 5$  cm<sup>2</sup> (FWHM<sup>2</sup>). The efficiency has been evaluated considering a fiducial area of  $5 \times 5$  pads around the expected hit. At a gain of 5000 the DRL shows an efficiency of 98%, while the SG1 and SG2 achieve a detection efficiency of 78% and 95% respectively, larger than their geometrical acceptance. The SG2++ tends to an almost full efficiency of about 97%.

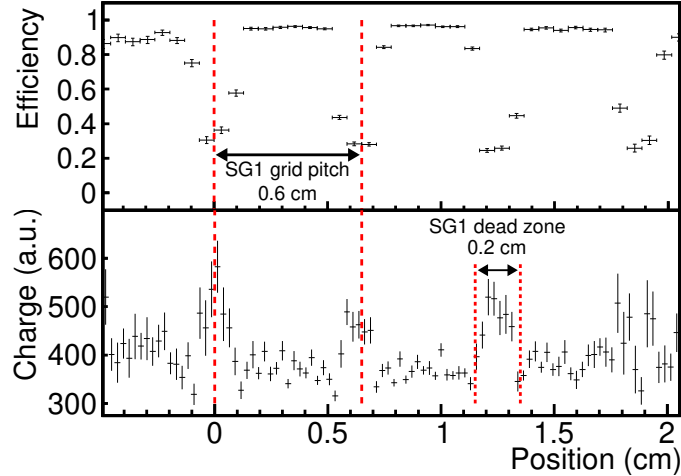


**Figure 12.** Efficiency and charge profile for the SG1 layout measured at CERN. Visible its geometrical features: the 2 mm wide dead zones and the 6 mm grid pitch.

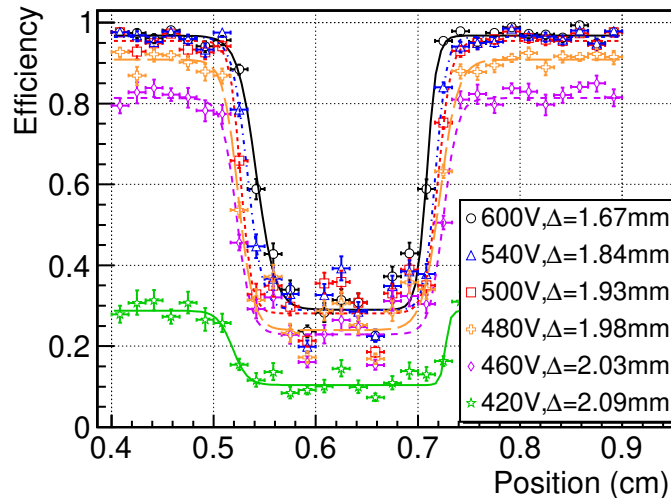


**Figure 13.** Zoom of the efficiency profile in the dead zone for different voltages for SG1. The  $\Delta$  is the difference between the inflection points of the two fitting Fermi-Dirac functions.

We have investigated this effect, typical of detectors with GEM-like amplification stage [11, 12], reporting as example the efficiency and the charge profile for the SG1. In figure 12 (top) we plot the efficiency and in figure 12 (bottom) the charge as a function of the incidence point reconstructed by the GEM trackers. The geometrical structure of the detector layout is visible on both: an efficiency drop and an increase of the charge are present in correspondence of the dead zones. Actually the wells close to the dead zones collect also the primary ionization produced above the inefficient regions (*focusing effect*) resulting in a recovery of the detection efficiency; at the same time the amplification in these wells is increased probably due to the squeezing of the drift field lines. Moreover, as shown in figure 13, increasing the HV applied to the amplification stage the efficiency in the dead zone improves, as observed in GEM detectors (KLOE-2 CGEM [14]).

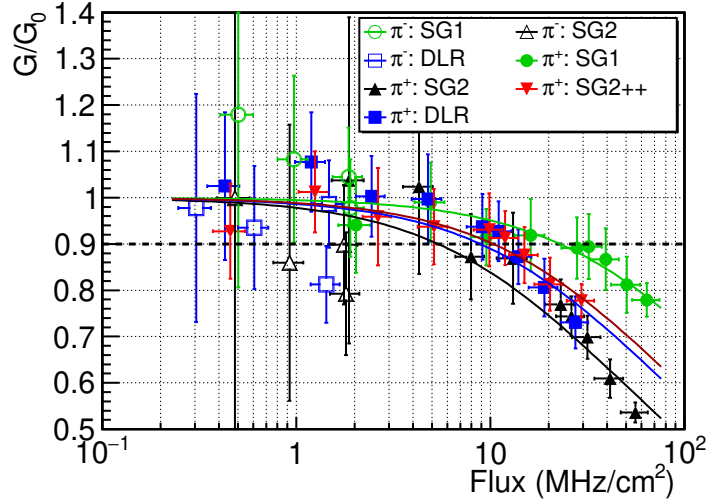


**Figure 14.** Normalized gas gain for the HR-layouts as a function of the pion flux. The function used to fit the points is the one derived in [1].

## 4.2 Rate capability measurement

The rate capability of the HR-layouts has been measured at the PSI  $\pi$ M1 facility that provides a quasi-continuous high-intensity secondary beam with a fluence of  $\sim 10^7$   $\pi^-/s$  and  $\sim 10^8$   $\pi^+/s$ , for a momentum ranging between 270÷350 MeV/c. This measurement can be considered reliable because the dimension of the average beam spot is larger than the basic cells of all the HR prototypes. The result of this study is reported in figure 14.

The low rate measurements ( $\leq 1$  MHz/cm<sup>2</sup>) have been performed with the  $\pi^-$  beam, while the high intensity have been obtained with the  $\pi^+$  beam. The detectors have been operated at a gain of about 5000. The particle rate has been estimated with the current drawn by the GEM, that owns a linear behaviour up to several tens of MHz/cm<sup>2</sup> [15]. The beam spot has been evaluated with a 2-D gaussian fit of the hits reconstructed on the X-Y plane for each detector.

The gain drop observed at high particle fluxes is correlated with the ohmic behaviour of the detectors due to the DLC film. The larger the radiation rate, the higher is the current drawn through the resistive layer and, as a consequence, the larger the drop of the amplifying voltage.

The different behaviours of the HR-layouts depend on their resistivity and current evacuation scheme and then on the  $\Omega_{\text{eff}}$  (eq. (3.1)). As shown in figure 15, the rate capability decreases as the effective resistance increases. In particular the HR-layouts corresponding to  $\Omega_{\text{eff}} \approx 200$  M $\Omega$  stand particle fluxes ranging from 6 to 10 MHz/cm<sup>2</sup> with high detection efficiency.

## 4.3 Discharge studies

The radiation rate at PSI allows a dedicated study on the discharges occurrence and their amplitude. We have used for the test a 270 MeV/c  $\pi^+$  beam with a proton contamination of 3.5%. The beam intensity has been set  $\sim 90$  MHz on a  $\sim 5$  cm<sup>2</sup> spot.

The currents drawn by all the electrodes have been recorded every second and then analyzed, removing from the analysis the values corresponding to the beam-off periods. The average current at a gain of 5000 has been of the order few  $\mu$ A.

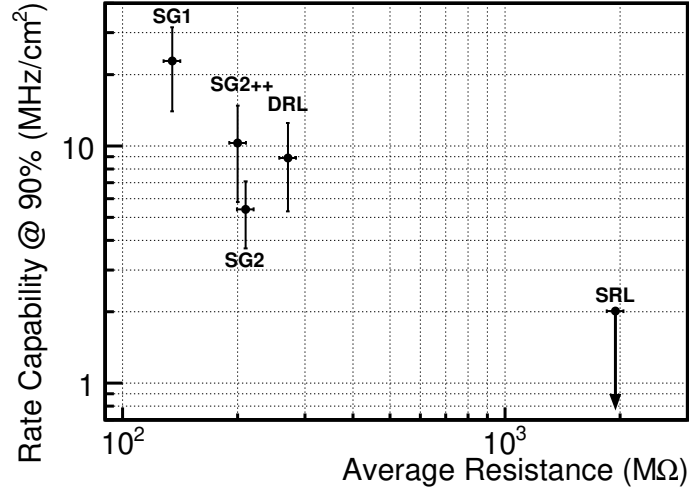


**Figure 15.** Rate capability at  $G/G_0 = 90\%$  as a function the effective resistance  $\Omega_{\text{eff}}$ . For the SRL, since the irradiation has not been uniform over the active area, we give an upper limit of its rate capability.

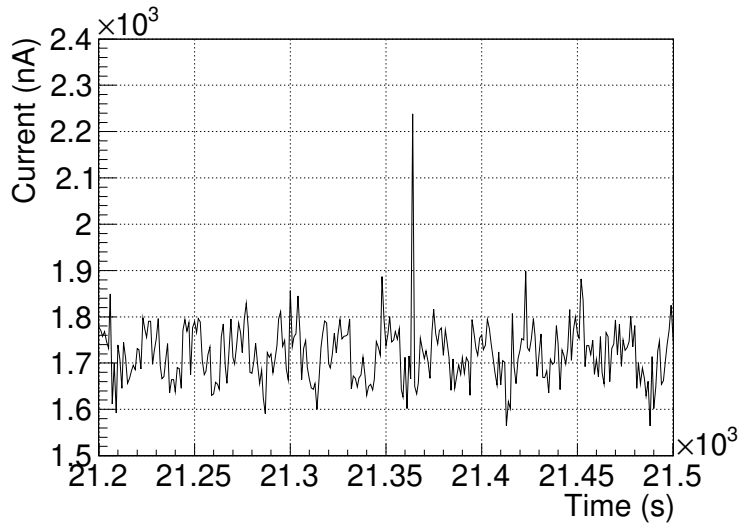


**Figure 16.** Typical current spike in a  $\mu$ -RWELL.

A spark has been defined as the current spike, figure 16, exceeding  $5\sigma$  the average current level due to the particle flux while its amplitude is the difference between the current peak and the reference current value. The spark probability per incident hadron is

$$P_{\text{spark}} = \frac{N_{\text{spark}}}{R \times \Delta t \times S}$$

where  $R$  is the particle rate,  $\Delta t$  is the irradiation time and  $S$  is the spot area ( $\text{FWHM}^2$ ).

As shown in figure 17, the  $P_{\text{spark}}$  for a  $\mu$ -RWELL (full circle) is slightly lower than the one measured for triple-GEM (full square). In the plot we have reported also measurements done in the 2004 in the framework of the R&D for LHCb (open square) [15] with triple-GEMs flushed with the same gas mixture. These points have been renormalized to the beam conditions of 2018 by

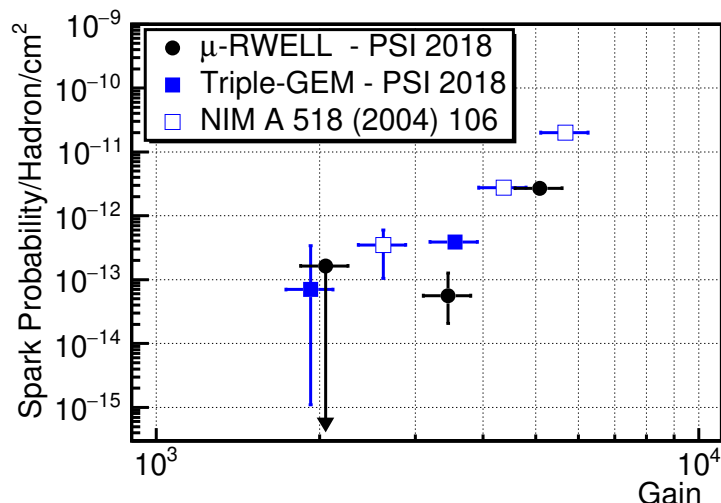


**Figure 17.** Spark probability per incident particle averaged on the six  $\mu$ -RWELL detectors compared with GEM. The measurements at the lowest gain suffers of lack of statistics: in particular for  $\mu$ -RWELL since no sparks have been detected the point represents an upper limit.

**Table 2.** Parameters of the discharge measurements done with GEM in 2004 and in 2018.

	2004	2018
proton contamination	7%	3.5%
drift gap thickness	3 mm	6 mm
beam momentum	300 MeV/c	270 MeV/c
proton specific ionization	950 e-I/cm	1090 e-I/cm

re-scaling the gain of a factor 2.29, due to the different specific ionization and to the thickness of the drift gap, and the  $P_{\text{spark}}$  of a factor 0.5 because of the different proton contamination (see table 2).

In figure 18 we report the distributions of the spark amplitude measured in one of the external trackers and in the six  $\mu$ -RWELLS. Taking into account the different gains (see the legend) this plot suggests that the spark amplitude for the  $\mu$ -RWELL is moderately lower than for triple-GEM.

During the irradiation test at PSI each detector has integrated a charge of the order 100 mC/cm<sup>2</sup> (in 42 hours) without showing any performance degradation. This result, confirmed by the exposure at GIF++ facility (180 mC/cm<sup>2</sup> in 250 days), should be compared with the expected 600 mC/cm<sup>2</sup> in 1 year of operation (10<sup>7</sup>s) in the M2R1 HL-LHCb muon station.

## 5 Conclusions

In this paper we have discussed different resistive layouts of  $\mu$ -RWELL for high rate applications. The prototypes have been tested up to particle fluxes exceeding 20 MHz/cm<sup>2</sup> at the  $\pi$ M1 beam facility of the PSI.

Among the proposed layouts different solutions have been found that satisfy the very stringent requirements for the detectors in view of the phase-2 upgrades of muon apparatus at the HL-LHC as well as in the apparatus at the future accelerators FCC-ee/hh and CepC.

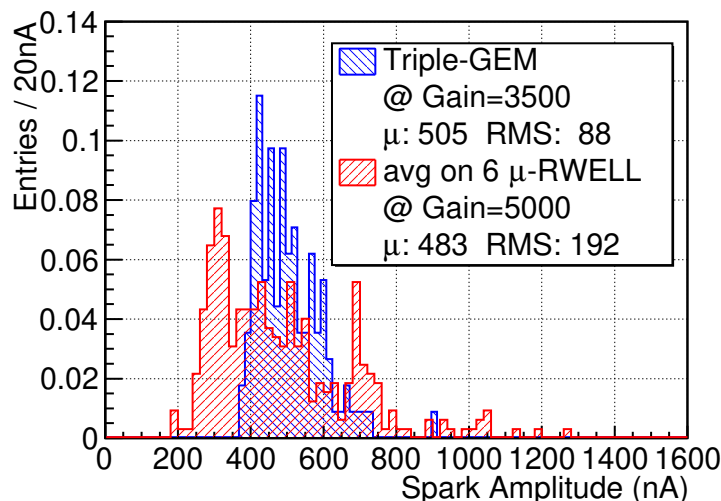


**Figure 18.** Spark amplitude comparison among the GEM and the six  $\mu$ -RWELL detectors. The  $\mu$ -RWELL have been operated at higher gain than GEM.

A rate capability up to  $10 \text{ MHz/cm}^2$  with a detection efficiency of the order of  $97\div 98\%$  are the performance achievable with the proposed technologies.

In addition, it must be stressed that the SG2++ layout, based on DLC+Cu sputtered Apical<sup>®</sup> foils, can be manufactured with full sequential-build-up technology, thus allowing a straightforward technology transfer of the manufacturing process to the industry.

The presence of the resistive layer helps to quench the spark amplitude, suppressing the transition from streamer to discharge. The probability and the amplitude of the sparks for  $\mu$ -RWELL result to be slightly lower than the one from triple-GEMs.

## Acknowledgments

We would like to acknowledge Dr Zhou Yi for his contribution in preparing the DLC+Cu sputtered Apical<sup>®</sup> foils used for the manufacturing of the improved SG2++ prototypes. The project has been funded from the European Union’s Horizon 2020 Research and Innovation program under Agreement n<sup>o</sup> 654168-AIDA2020.

## A A model for HR-layouts

According to the model reported in appendix B of [1], proposed by one of the authors (G. Morello), in a squared SRL detector of size  $d$  (figure 19), the charge produced at its center experiences, moving toward the ground, an average resistance  $\Omega_{\text{SRL}} \propto \rho d/2$ .

Assuming the same conditions, in particular the resistivity  $\rho$ , in a DRL detector that, whatever the size, owns a vias density of  $1 \text{ cm}^{-2}$ , the average resistance seen by the charge produced in the center of a matrix cell is  $\Omega_{\text{DRL}} \propto \rho 1.5$ , where the factor 1.5 averages the path on the two resistive layers.

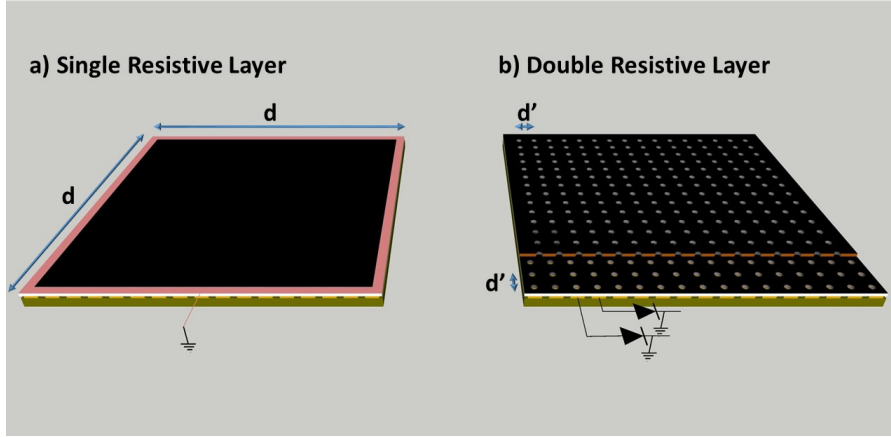


**Figure 19.** The charge evacuation scheme of the SRL compared to DRL.

The ratio between the two values becomes smaller as  $d$  increases. In particular assuming  $d' = 1$  cm and  $d = 10$  cm, i.e. the size of the SRL used in the tests, the ratio is

$$\frac{\Omega_{\text{DRL}}}{\Omega_{\text{SRL}}} = \frac{\rho (d' + d'/2)}{\rho d/2} = \frac{1.5}{5} = 0.3$$

The rate capability depends on the inverse of the  $\Omega$ , so in this example for the DRL it can be expected  $\sim 3$  times larger than for the SRL.

To be strongly remarked that this relation stands for point-like irradiation at the center of the basic cell (i.e. X-rays) and it has been considered for the developments of the HR-layouts.

We want to stress that this  $\Omega$  is different from the  $\Omega_{\text{eff}}$  cited in the text defined for a total irradiation of the basic cell.

## References

- [1] G. Bencivenni, R. De Oliveira, G. Morello and M.P. Lener, *The micro-Resistive WELL detector: a compact spark-protected single amplification-stage MPGD*, 2015 *JINST* **10** P02008 [[arXiv:1411.2466](https://arxiv.org/abs/1411.2466)].
- [2] M.S. Dixit and A. Rankin, *Simulating the charge dispersion phenomena in micro pattern gas detectors with a resistive anode*, *Nucl. Instrum. Meth. A* **566** (2006) 281 [[physics/0605121](https://arxiv.org/abs/physics/0605121)].
- [3] G. Bencivenni et al., *Performance of  $\mu$ -RWELL detector vs resistivity of the resistive stage*, *Nucl. Instrum. Meth. A* **886** (2018) 36.
- [4] V. Parkhomchuck, Y. Pestov and N. Petrovykh, *A spark counter with large area*, *Nucl. Instrum. Meth.* **93** (1971) 269.
- [5] R. Santonico and R. Cardarelli, *Development of Resistive Plate Counters*, *Nucl. Instrum. Meth. A* **187** (1981) 377.
- [6] M. Anelli, G. Bencivenni, G. Felici and L. Magro, *Glass electrode spark counters*, *Nucl. Instrum. Meth. A* **300** (1991) 572.
- [7] P. Fonte et al., *Advances in the Development of Micropattern Gaseous Detectors with Resistive Electrodes*, *Nucl. Instrum. Meth. A* **661** (2012) S153 [[arXiv:1005.1477](https://arxiv.org/abs/1005.1477)].



- [8] A. Ochi et al., *Carbon sputtering Technology for MPDG detectors*, *PoS(TIPP2014)* 351 (2014).
- [9] G. Morello et al., *Advances on micro-RWELL gaseous detector*, *PoS(BORMIO2017)*002 (2017).
- [10] Y. Zhou et al., *News on DLC Coatings*, contribution to *The RD51 Collaboration Meeting and the topical workshop on MPGD Stability*, 18–22 June 2018, Technical University of Munich, Munich, Germany [<https://indico.cern.ch/event/709670/timetable/#20180622.detailed>].
- [11] G. Bencivenni et al., *A triple GEM detector with pad readout for high rate charged particle triggering*, *Nucl. Instrum. Meth. A* **488** (2002) 493.
- [12] C. Richter, A. Breskin, R. Chechik, G. Garty and A. Sharma, *Absolute electron transfer efficiency of GEM*, *Nucl. Instrum. Meth. A* **461** (2001) 38.
- [13] M. Raymond et al., *The APV25 0.25 m CMOS readout chip for the CMS tracker*, *IEEE Nucl. Sci. Symp. Conf. Rec.* **2** (2000) 9/113.
- [14] A. Balla et al., *The KLOE-2 Inner Tracker: Detector commissioning and operation*, *Nucl. Instrum. Meth. A* **845** (2017) 266.
- [15] V. Ableev et al., *TPG development*, *Nucl. Instrum. Meth. A* **518** (2004) 113.